Two-Dimensional Topological Polariton Laser

Yaroslav V. Kartashov[1,2] and Dmitry V. Skryabin[3]
[1]ICFO-Institut de Ciencies Fotoniques, The Barcelona Institute of Science and Technology, 08860 Castelldefels (Barcelona), Spain
[2]Institute of Spectroscopy, Russian Academy of Sciences, Troitsk, Moscow, 108840, Russia
[3]Department of Physics, University of Bath, BA2 7AY, Bath, United Kingdom

(Received 17 September 2018; revised manuscript received 4 December 2018; published 26 February 2019)

We provide proof-of-principle illustration of lasing in a two-dimensional polariton topological insulator. Topological edge states may arise in a structured polariton microcavity under the combined action of spin-orbit coupling and Zeeman splitting in the magnetic field. Their properties and lifetime are strongly affected by gain. Thus, gain concentrated along the edge of the insulator can counteract intrinsic losses in such a selective way that the topologically protected edge states become amplified, while bulk modes remain damped. When gain is compensated by nonlinear absorption the metastable nonlinear edge states are formed. Taking a triangular structure instead of an infinite edge we observed persistent topological currents accompanied by the time-periodic oscillations of the polariton density.

DOI: 10.1103/PhysRevLett.122.083902

The physics of topological insulators is an interdisciplinary research area promising numerous applications [1,2]. Topological insulators behave as usual insulators in their bulk, but allow topologically protected unidirectional edge currents with in-gap energies. They were initially studied in electronic systems [1–4], but later on they have been introduced in mechanical [5], acoustic [6,7], atomic [8–11], and photonic systems [12–24]. The latter include gyromagnetic photonic crystals [12,13], arrays of coupled resonators [15–17], metamaterials [18,19], helical waveguide arrays [20–23], and microcavity polaritons [24–27]. Some of these systems, in contrast to electronic ones, allow investigation of the interplay between topology and nonlinearity [28], leading to such new phenomena as inversion of velocity of the edge states [29,30], modulational instability [31,32], formation of solitons [33–37] and vortices [38], the effects of bistability [39] and nonlinear isolation [40].

Most of topological systems feature intrinsic losses [41]. Spatially inhomogeneous losses can be used for observation of topological defect states [42–44], but in general losses are detrimental for observation and practical utilization of topological states, thus gain compensating them is required. This is where the topological nature of the system becomes truly beneficial, since the parameters of the system can be engineered to allow preferential amplification of strongly localized topological states relative to the other. Lasers based on this approach were realized in one-dimensional photonic and polaritonic structures [45–48]. It was also used for observation of lasing in topological photonic crystals [49] and lattices of coupled-ring resonators [50,51]. Topological insulator lasers are resistant to disorder limiting performance of conventional lasers.

The aim of this work is to show that a *two-dimensional* topological insulator laser supporting persistent edge currents, which do not exist in one-dimensional systems [46], can be realized using microcavity polaritons—a promising platform for the exploration of topological effects. Existing technologies of microcavity structuring [52,53] allow fabrication of periodic systems exhibiting required degeneracies in the linear spectrum [54–58]. Opening of the topological gaps in these structures occurs due to simultaneous action of the polarization-dependent tunneling between pillars, which is producing the effective spin-orbit coupling effect [59–61], and Zeeman splitting of the polariton spectra. Isolated microcavity pillars [62,63], planar structures [64], and organic microcavities [65] were used for demonstration of polariton lasing, where linear gain is compensated by nonlinear absorption required for steady-state laser operation [66–68].

Below we consider polariton lasing in the presence of spin-orbit coupling and Zeeman splitting in a honeycomb lattice, where gain is localized only along the lattice edges. Such gain in the system with broken time-reversal symmetry results in preferential amplification of unidirectional edge states. Very high (in comparison with photonic systems [49]) repulsive nonlinearity stemming from exciton-exciton interactions allows realization of new regimes of lasing; it can cause dynamical instabilities of edge states and even transitions between states from different topological gaps. Developed technologies of microcavity structuring allow design of new practically sized laser structures, such as triangular ones, where instabilities are suppressed and persistent edge currents form.

We model the topological polariton laser using the system of coupled nonlinear Schrödinger equations for

spin-positive and spin-negative components of the spinor wave function $\Psi = (\psi_+, \psi_-)^T$ [29,53,66–68]:

$$i\partial_t\psi_\pm = -(1/2)(\partial_x^2 + \partial_y^2)\psi_\pm + \beta(\partial_x \mp i\partial_y)^2\psi_\mp + [\mathcal{R}_{\rm re}(x,y) + i\mathcal{R}_{\rm im}(x,y) - i\gamma \pm \Omega]\psi_\pm + [(1 - i\alpha)|\psi_\pm|^2 + \sigma|\psi_\mp|^2]\psi_\pm. \quad (1)$$

We assume that the polariton condensate is created by the optically injected excitons that generate a reservoir of active excitons pumping the polariton condensate, see, e.g., Refs. [69,70]. For the sake of simplicity, we adiabatically eliminate the rate equation for the reservoir as has been done by many authors, see, e.g., Refs. [67,71]. We use circular polarization basis with wave functions $\psi_\pm$ for spin-positive and spin-negative polaritons; spin-orbit coupling is described by the β terms [59–61]; Ω is proportional to the Zeeman energy splitting in the external magnetic field; we assume repulsion for polaritons of the same spin and weak ($\sigma \sim -0.05$) attraction for polaritons with opposite spins [72]; nonlinear absorption $\sim\alpha$ and linear losses $\sim\gamma$. The honeycomb lattice is described by the potential energy term $\mathcal{R}_{\rm re}(x,y) = -p_{\rm re}\sum_{n,m}\mathcal{Q}(x - x_n, y - y_m)$, where potential wells have the depth $p_{\rm re}$ and shapes $\mathcal{Q}=\exp[-(x^2+y^2)/d^2]$ with width d and separation a. The lattice is truncated by the zigzag edges in the x direction and is periodic in y with a period $Y = 3^{1/2}a$ [Fig. 1, top left]. Gain acts only inside the edge pillars, which can be achieved with focused beam illuminating edge channels [73], and is accounted using the imaginary part $\mathcal{R}_{\rm im}(x,y) = p_{\rm im}\sum_{q,l}\mathcal{Q}(x - x_q, y - y_l)$ of the potential, with $p_{\rm im} \ll p_{\rm re}$ being gain amplitude [Fig. 1, top right]. We normalize x, y coordinates to the characteristic distance L, all energy parameters $(p_{\rm re}, \Omega)$ to $\varepsilon_0 = \hbar^2/mL^2$, where m is the effective polariton mass, and time to $\tau_0 = \hbar\varepsilon_0^{-1}$. For $L = 1$ μm and $m \sim 10^{-34}$ kg, we get $\varepsilon_0 \sim 0.7$ meV and $\tau_0 \sim 0.9$ ps. We assume [69,73,27] width of the Gaussian potential wells of 1 μm ($d = 0.5$), pillar-to-pillar separation of 1.4 μm ($a = 1.4$), potential depth ~5.6 meV ($p_{\rm re} = 8$), Zeeman splitting of 0.35 meV ($\Omega = 0.5$), spin-orbit coupling energy of ~0.2 meV ($\beta = 0.3$), and characteristic polariton lifetime ~18 ps ($\gamma = 0.05$). Structure with bearded edges is discussed in Ref. [74].

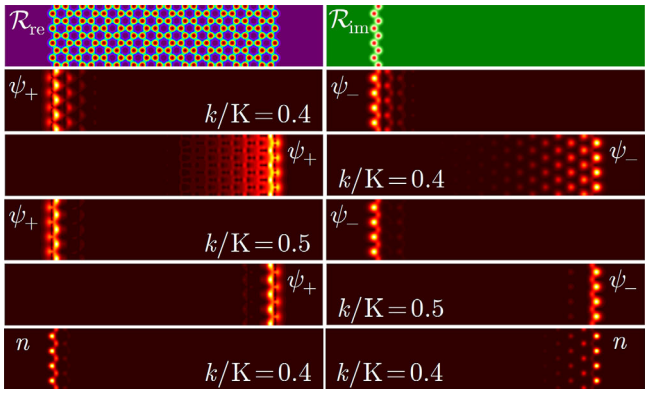

FIG. 1. Lattice potential and profile of the gain concentrated at the left edge of the polariton insulator (1st row). $|\psi_\pm|$ distributions in the counterpropagating edge states from two different branches at $k/K = 0.4$ (2nd, 3rd rows) and $k/K = 0.5$ (4th, 5th rows), $p_{\rm im} = 0.13$. Density distributions $n = |\psi_+|^2 + |\psi_-|^2$ in two states at $k/K = 0.4$ are shown in the 6th row. Since gain acts on the left edge, the states from the left edge are amplified, and the right edge states decay.

Bulk honeycomb potentials are known to possess degeneracies in the mode spectrum around Dirac $\mathcal{K}$ and $\mathcal{K}'$ points. Simultaneously acting spin-orbit coupling and Zeeman splitting break time-reversal symmetry of Eq. (1) and lead to a topological gap opening around Dirac points (several gaps may open for our β, Ω parameters). Topological properties of this system are characterized by topological invariants—band Chern numbers. Using the approach of Ref. [37] we calculated Chern numbers for top four bands: $\mathcal{C}_1 = -1$, $\mathcal{C}_2 = 0$, $\mathcal{C}_3 = +1$, and $\mathcal{C}_4 = 0$. This structure of topological invariants is due to the spinor character of our system, whose spectrum at $\beta = 0$ includes two mutually shifted by 2Ω groups of bands, where either the ψ_+ or ψ_- component dominates [35]. Some of them (including bands touching in Dirac points) overlap and may fold for nonzero spin-orbit coupling β. When the lattice is truncated linear edge states appear in topological gaps. To find them we omit nonlinear terms in Eq. (1), while keeping linear losses and gain, and search for eigenmodes $\psi_\pm(x,y,t) = u_\pm(x,y)\exp(iky + i\varepsilon t)$, where $u_\pm(x,y) = u_\pm(x, y+Y)$ and $u_\pm(x \to \pm\infty, y) = 0$, k is the Bloch momentum along the y direction, and $\varepsilon = \varepsilon_{\rm re} + i\varepsilon_{\rm im}$ is the "energy", which is a complex number in our case due to presence of gain and losses (modes with $-\varepsilon_{\rm im} > 0$ are amplified, while modes with $-\varepsilon_{\rm im} < 0$ are attenuated; for $p_{\rm im} = 0$ all modes are attenuated and $\varepsilon_{\rm im} \equiv \gamma$). Figure 2 shows $\varepsilon_{\rm re}, \varepsilon_{\rm im}$ versus

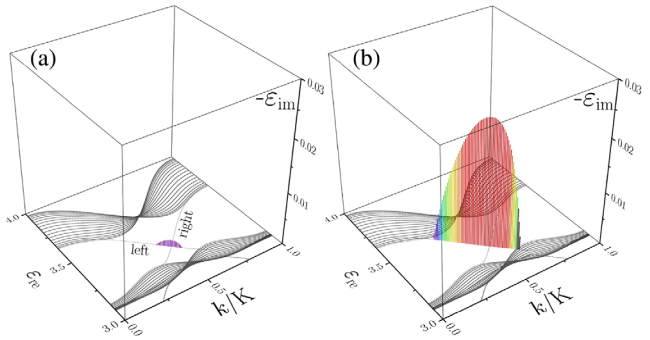

FIG. 2. Real part $\varepsilon_{\rm re}$ and imaginary part $\varepsilon_{\rm im}$ (taken with opposite sign) of energies of linear modes in polariton topological insulator with amplification on its left edge versus k/K at $p_{\rm im} = 0.09$ (a) and $p_{\rm im} = 0.13$ (b). Captions in (a) indicate the edge at which the edge state resides. Only modes with $-\varepsilon_{\rm im} > 0$ (shown by colored bars) experience amplification (lase). Note, that all the values of $\varepsilon_{\rm im}$ with $-\varepsilon_{\rm im} < 0$ are set to zero.

normalized Bloch momentum k/K, where $K = 2\pi/Y$. The dependence $\varepsilon_{\mathrm{re}}(k)$ reveals edge states in topological gaps. The number of edge states per interface is defined by the gap Chern number (sum of Chern numbers for all bands lying above this gap). It is -1 for two upper gaps (second gap is shown in Fig. 2 only partially, see [74] for extended spectrum). Usually edge states connecting bands emerge from them around $k = K/3$ and $k = 2K/3$ points—remnants of $\mathcal{K}$ and $\mathcal{K}'$ points in the spectrum of bulk lattice (intervals of edge state existence may be asymmetric around $k = K/2$ point due to spin-orbit coupling).

Edge states with $\partial\varepsilon_{\mathrm{re}}/\partial k > 0$ (corresponding to the current in the negative y direction) reside on the right edge, while states with $\partial\varepsilon_{\mathrm{re}}/\partial k < 0$ (current in the positive y direction) reside on the left edge. Edge states may emerge in some lower gaps, but they do not lase for our parameters and are not described here.

Efficiency of the pump going into the edge and other possible states from the edge pillars depends on the overlap of a given state with the amplifying pillars. Main advantage of our system is that topological edge states are amplified most efficiently among all modes of the system. As a result when gain amplitude p_{im} exceeds a threshold $p_{\mathrm{im}}^{\mathrm{th}} \sim 0.088$ some topological modes at the edge where gain acts acquire energies with $-\varepsilon_{\mathrm{im}} > 0$ and start to lase [colored bars in Fig. 2(a)]. In the upper topological gap shown in Fig. 2, lasing of the edge states becomes possible first around the momentum $k = K/2$. For selected Ω, β parameters lasing may occur also in second gap around $k = 0$ (Fig. S1 in the Supplemental Material [74]), but usually it requires slightly larger gain amplitude than the threshold value mentioned above. The momentum range where lasing occurs expands with p_{im} [Fig. 2(b)]. For sufficiently large gain lasing can also happen for the bulk modes, but the topological modes feature the lowest threshold. Examples of the linear edge states are shown in Fig. 1. Gain acting only on one of the two edges leads to grows of modes on that edge and lifts the degeneracy of the edge states at $k = K/2$ (4th and 5th rows in Fig. 1). Since edge state existence interval is asymmetric with respect to $k = K/2$, at fixed k the energies $\varepsilon_{\mathrm{re}}$ of two states from different braches have different separations from gap edges, leading to different localization of modes (localization is larger for $\varepsilon_{\mathrm{re}}$ values closer to the gap center).

Linear amplification of the edge states on the left boundary for $p_{\mathrm{im}} > p_{\mathrm{im}}^{\mathrm{th}}$ can be balanced by the nonlinear absorption (pump depletion), and lead to formation of stable lasing states. We seek such solutions of Eq. (1) in the form $\psi_{\pm}(x, y, t) = u_{\pm}(x, y)\exp(iky + i\mu t)$, where k is the momentum and μ is the real parameter characterizing the energy (or frequency) shift, $u_{\pm}(x, y) = u_{\pm}(x, y + Y)$ is the periodic function. The latter has been found using Newton iterations with an additional power balance condition allows us to calculate μ. Nonlinear modes emerge when gain exceeds lasing threshold for a given k, see Fig. 3(a), where we show the dependence of the maximal

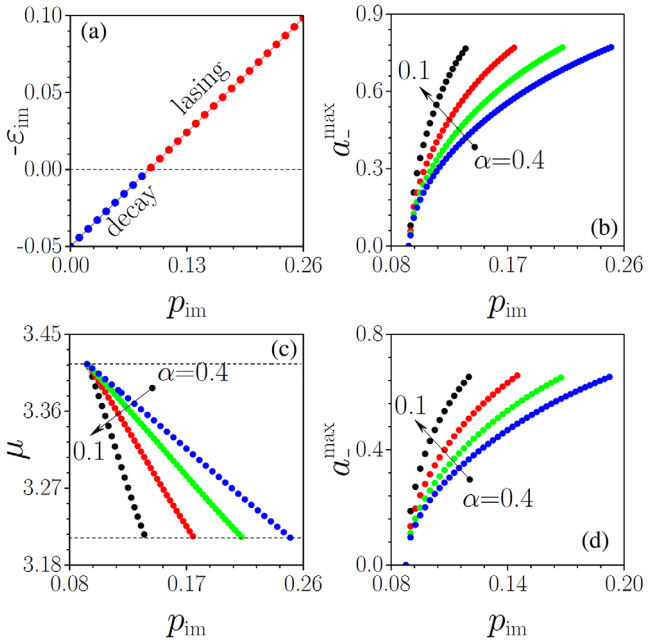

FIG. 3. (a) Maximal attenuation or gain experienced by the linear edge state (imaginary part of its energy $-\varepsilon_{\mathrm{im}}$) versus p_{im}. At $p_{\mathrm{im}} \approx 0.09$ decay is replaced by amplification leading to lasing in edge states. Peak amplitude of dominating ψ_- component (b) and energy (c) of stationary nonlinear edge state with $k = 0.4K$ versus p_{im} for $\alpha = 0.1$, 0.2, 0.3, and 0.4. Upper dashed line in (c) is the energy of linear edge state; lower dashed line is the edge of the topological gap at $k = 0.4K$. (d) The same as in (b) but for $k = 0.5K$. In all cases gain acts on the left edge.

gain $-\varepsilon_{\mathrm{im}}$ experienced by linear mode on p_{im} at $k = 0.4K$. Figures 3(b), 3(d) show that peak amplitude $a_-^{\max}$ of the dominating ψ_- component in the *nonlinear* edge state (see examples of profiles in Fig. 5) increases with p_{im}. The energy μ of the nonlinear edge state at its generation threshold (bifurcation point) coincides with that of the linear mode, $\varepsilon_{\mathrm{re}}$ [top dashed line in Fig. 3(c)], and decreases with the increasing gain, until it reaches at certain critical p_{im} the lower boundary of topological gap (lower dashed line), below which edge states couple with delocalized bulk modes acquiring nonzero background inside the array. We truncated respective $a_-^{\max}(p_{\mathrm{im}})$ dependencies at this critical value even though they can formally be continued beyond it. An interval of gain corresponding to the edge state energy located within the topological gap expands with increase of the nonlinear absorption [Fig. 3(b)].

Nonlinear edge states demonstrate several destabilization scenarios and resulting dynamical evolution. For the gain levels close to the lasing threshold, the edge modes are practically stable. They do not show instabilities even at $t \sim 10^4$ exceeding polariton lifetime by several orders of magnitude. Evolution of peak amplitude of perturbed metastable state is shown in Fig. 4(a), while corresponding density distribution at large time is illustrated in Fig. 5(c). Large-amplitude edge states with energies μ close to the

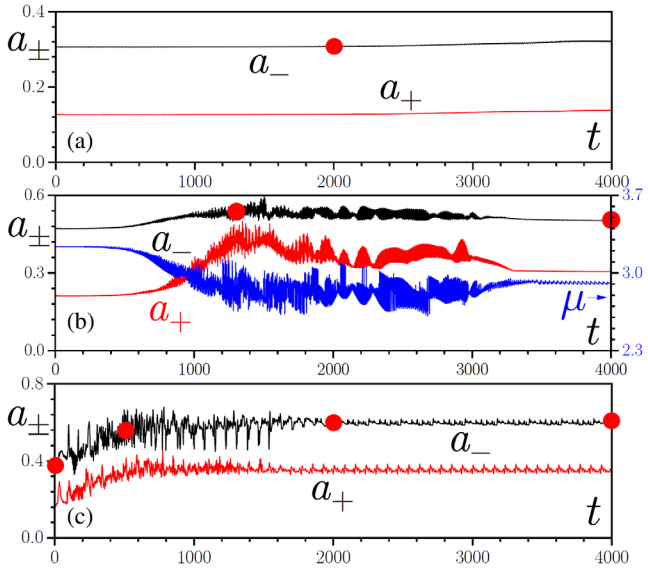

FIG. 4. Peak amplitudes of ψ_+ and ψ_- components versus time illustrating (a) metastable evolution at $p_{\rm im} = 0.11$, $\alpha = 0.4$, $k = 0.5K$, (b) transformation of the unstable edge state into stable one at $p_{\rm im} = 0.14$, $\alpha = 0.4$, $k = 0.5K$ [blue line shows instantaneous $\mu(t)$ dependence], and (c) excitation of the persistent current in triangular structure at $p_{\rm im} = 0.13$, $\alpha = 0.4$, $k = 0.4K$. Dots correspond to patterns shown in Figs. 5 and 6.

border of the topological gap, obtained at high gain levels are unstable, see Fig. 4(b). However, even in the developed instability regime the wave remains localized close to the lattice edge, see Fig. 5(d), and the radiation emitted in the course of instability development into the lattice bulk is quickly absorbed. After some transient stage this wave transforms into a stable pattern from Fig. 5(e) with distinct spatial spectrum [compare input and output stripe-like spectra in Fig. 5(f) and 5(g) that show notable mutual shift], that has lower energy $\mu \sim 2.9$ as follows from instantaneous $\mu(t)$ dependence in Fig. 4(b); i.e., this stable state originates from the lower topological gap. Increasing the nonlinear absorption coefficient to $\alpha \sim 1$ tends to suppress instabilities and leads to formation of the breathing edge states.

To prove that edge currents in our system are topologically protected we consider interaction of the nonlinear edge states with defect in the form of missing pillar [Fig. 5(h),5(i)]. When $\beta, \Omega \neq 0$ edge state is only locally deformed around defect, revealing persistent current [Fig. 5(j)]. If we make system nontopological, e.g., by setting spin-orbit coupling β to zero, the edge states exhibit strong deformation extending far beyond the defect indicating on considerable reduction of lasing intensity [Fig. 5(k)]. Moreover, ψ_+ and ψ_- components in such state become identical at large t leading to loss of polarization structure (see Fig. S2 in [74] for comparison of local polarization degrees in states with nonzero and zero β) typical for topological edge states [39].

Spatially periodic nonlinear waves in conservative or dissipative systems often become unstable with respect to perturbations containing spatial frequencies from certain finite band, see, e.g., Refs. [35,75]. On the other hand, the size of the system imposes the restriction on the minimal spatial frequency of a perturbation that can be considered practical. Therefore, in a finite system the instability band is limited not only on the side of high spatial frequencies, but also on the low-frequency side, and it can even vanish completely making the wave stable. To test this hypothesis in polariton topological insulators, we considered triangular insulator with gain on its edges, depicted in Fig. 6. We took as an input at $t = 0$ the exact nonlinear edge state at $k = 0.4K$ obtained for the straight edge for the same $p_{\rm im}, \alpha$ and imposed a broad envelope on it to excite one side of the triangle. After a transient stage, where clockwise circulation is already obvious, one observes formation of the

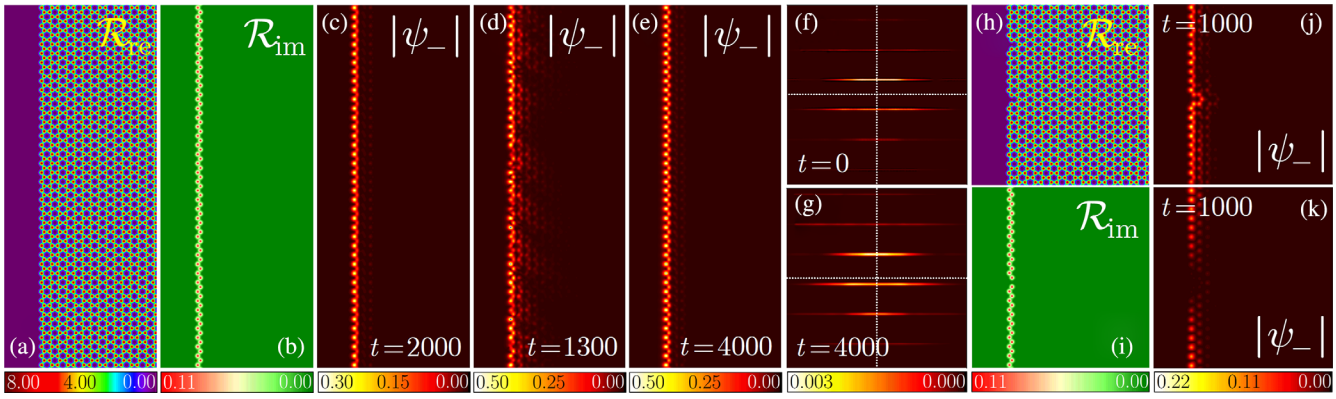

FIG. 5. (a) Potential and (b) gain profile in polariton topological insulator. (c) $|\psi_-|$ distribution in metastable perturbed edge state at $p_{\rm im} = 0.11$, $t = 2000$. (d), (e) Decay of the unstable edge state and its transformation into stable one at $p_{\rm im} = 0.14$. (f), (g) Corresponding input and output spectra of ψ_- within $k_{x,y} \in [-3K, +3K]$ window, dashed lines show k_x, k_y axes. (h),(i) Potential and gain profile in insulator with a defect. Interaction of edge state with a defect in topological insulator with $\beta = 0.3$ (j) and in trivial insulator with $\beta = 0$ (k). In all cases $\alpha = 0.4$, $k = 0.5K$.

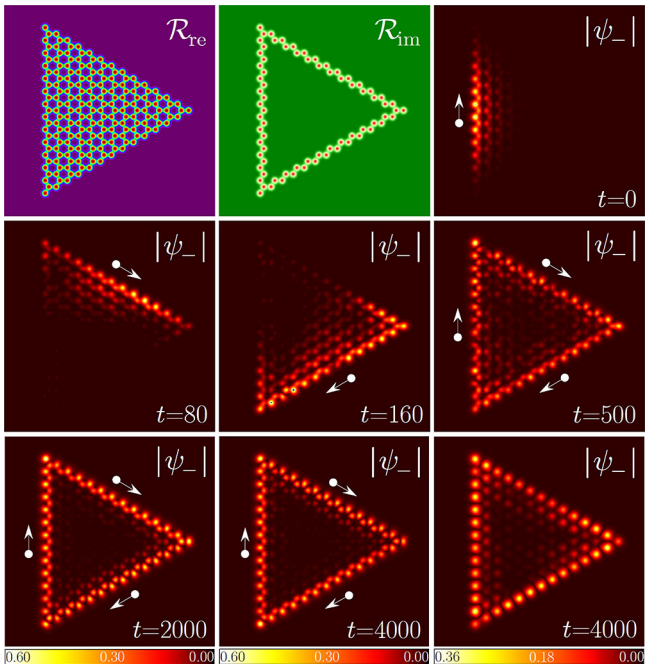

FIG. 6. Excitation of persistent surface current in triangular polariton laser at $p_{\rm im} = 0.13$, $\alpha = 0.4$, $\beta = 0.3$. Gain is provided on the edge of the entire triangular structure (see top row). Arrows indicate current direction. Bottom right panel: pattern excited in trivial insulator at $\beta = 0$.

persistent clockwise edge current (for different inputs) associated with the stable lasing regime. The peak amplitude of the wave exhibits small periodic oscillations [Fig. 4(c)]. The existence of the clockwise current is obvious also at large times, since modulus distribution in one region on the edge differs from that in other edge points, and this region travels along the edge. Corresponding spatial spectra [see the Supplemental Material [74], Figs. S3(a),3(b)] reveal practically absent contribution from $k_x, k_y = 0$ harmonics indicating the difference of this topological state from previously observed bulk modes [54]. Moreover, turning the system into a nontopological one by setting $\beta = 0$ drastically changes both spatial structure (see bottom right panel in Fig. 6, where only sites in one sublattice are populated in contrast to topological case) and spectrum [Fig. S2(c), Supplemental Material [74]] of the excited state.

Summarizing, we proposed a two-dimensional topological-insulator polariton laser. The system is based on a honeycomb array of microcavity pillars and allows us to realize lasing in the topologically protected edge states. We presented first examples of stable and unstable topological edge states in a polariton laser in an idealized geometry with the straight infinite edges and in a more a realistic triangular configurations. Our findings pave the way to experimental realizations of polaritonic topological lasers.

Y. V. K. acknowledges support from the Severo Ochoa program (SEV-2015-0522) of the Government of Spain, Fundacio Cellex, Fundació Mir-Puig, Generalitat de Catalunya and CERCA, as well as funding by RFBR and DFG according to the research Project No. 18-502-12080.

[1] M. Z. Hasan and C. L. Kane, Topological insulators, Rev. Mod. Phys. **82**, 3045 (2010).
[2] X.-L. Qi and S.-C. Zhang, Topological insulators and superconductors, Rev. Mod. Phys. **83**, 1057 (2011).
[3] F. D. M. Haldane, Model for a Quantum Hall Effect without Landau Levels: Condensed-Matter Realization of the "Parity Anomaly,", Phys. Rev. Lett. **61**, 2015 (1988).
[4] C.-Z. Chang *et al.*, Experimental observation of the quantum anomalous Hall effect in a magnetic topological insulator, Science **340**, 167 (2013).
[5] S. D. Huber, Topological mechanics, Nat. Phys. **12**, 621 (2016).
[6] Z. Yang, F. Gao, X. Shi, X. Lin, Z. Gao, Y. Chong, and B. Zhang, Topological Acoustics, Phys. Rev. Lett. **114**, 114301 (2015).
[7] C. He, X. Ni, H. Ge, X.-C. Sun, Y.-B. Chen, M.-H. Lu, X.-P. Liu, and Y.-F. Chen, Acoustic topological insulator and robust one-way sound transport, Nat. Phys. **12**, 1124 (2016).
[8] G. Jotzu, M. Messer, R. Desbuquois, M. Lebrat, T. Uehlinger, D. Greif, and T. Esslinger, Experimental realization of the topological Haldane model with ultracold fermions, Nature (London) **515**, 237 (2014).
[9] M. Aidelsburger, M. Lohse, C. Schweizer, M. Atala, J. T. Barreiro, S. Nascimbène, N. R. Cooper, I. Bloch, and N. Goldman, Measuring the Chern number of Hofstadter bands with ultracold bosonic atoms, Nat. Phys. **11**, 162 (2015).
[10] M. C. Beeler, R. A. Williams, K. Jimenez-Garcia, L. J. LeBlanc, A. R. Perry, and I. B. Spielman, The spin Hall effect in a quantum gas, Nature (London) **498**, 201 (2013).
[11] C. J. Kennedy, G. A. Siviloglou, H. Miyake, W. C. Burton, and W. Ketterle, Spin-Orbit Coupling and Quantum Spin Hall Effect for Neutral Atoms without Spin Flips, Phys. Rev. Lett. **111**, 225301 (2013).
[12] F. D. M. Haldane and S. Raghu, Possible Realization of Directional Optical Waveguides in Photonic Crystals with Broken Time-Reversal Symmetry, Phys. Rev. Lett. **100**, 013904 (2008).
[13] Z. Wang, Y. Chong, J. D. Joannopoulos, and M. Soljacic, Observation of unidirectional backscattering-immune topological electromagnetic states, Nature (London) **461**, 772 (2009).
[14] N. H. Lindner, G. Refael, and V. Galitski, Floquet topological insulator in semiconductor quantum wells, Nat. Phys. **7**, 490 (2011).
[15] M. Hafezi, E. A. Demler, M. D. Lukin, and J. M. Taylor, Robust optical delay lines with topological protection, Nat. Phys. **7**, 907 (2011).
[16] R. O. Umucalilar and I. Carusotto, Fractional Quantum Hall States of Photons in an Array of Dissipative Coupled Cavities, Phys. Rev. Lett. **108**, 206809 (2012).
[17] M. Hafezi, S. Mittal, J. Fan, A. Migdall, and J. M. Taylor, Imaging topological edge states in silicon photonics, Nat. Photonics **7**, 1001 (2013).

[18] A. B. Khanikaev, S. H. Mousavi, W.-K. Tse, M. Kargarian, A. H. MacDonald, and G. Shvets, Photonic topological insulators, Nat. Mater. **12**, 233 (2013).
[19] W.-J. Chen, S.-J. Jiang, X.-D. Chen, B. Zhu, L. Zhou, J.-W. Dong, and C. T. Chan, Experimental realization of photonic topological insulator in a uniaxial metacrystal waveguide, Nat. Commun. **5**, 5782 (2014).
[20] M. C. Rechtsman, J. M. Zeuner, Y. Plotnik, Y. Lumer, D. Podolsky, F. Dreisow, S. Nolte, M. Segev, and A. Szameit, Photonic Floquet topological insulators, Nature (London) **496**, 196 (2013).
[21] L. J. Maczewsky, J. M. Zeuner, S. Nolte, and A. Szameit, Observation of photonic anomalous Floquet topological insulators, Nat. Commun. **8**, 13756 (2017).
[22] S. Mukherjee, A. Spracklen, M. Valiente, E. Andersson, P. Öhberg, N. Goldman, and R. R. Thomson, Experimental observation of anomalous topological edge modes in a slowly driven photonic lattice, Nat. Commun. **8**, 13918 (2017).
[23] M. A. Bandres, M. C. Rechtsman, and M. Segev, Topological Photonic Quasicrystals: Fractal Topological Spectrum and Protected Transport, Phys. Rev. X **6**, 011016 (2016).
[24] A. V. Nalitov, D. D. Solnyshkov, and G. Malpuech, Polariton Z Topological Insulator, Phys. Rev. Lett. **114**, 116401 (2015).
[25] C.-E. Bardyn, T. Karzig, G. Refael, and T. C. H. Liew, Topological polaritons and excitons in garden-variety systems, Phys. Rev. B **91**, 161413(R) (2015).
[26] T. Karzig, C.-E. Bardyn, N. H. Lindner, and G. Refael, Topological Polaritons, Phys. Rev. X **5**, 031001 (2015).
[27] S. Klembt, T. H. Harder, O. A. Egorov, K. Winkler, R. Ge, M. A. Bandres, M. Emmerling, L. Worschech, T. C. H. Liew, M. Segev, C. Schneider, and S. Höfling, Exciton-polariton topological insulator, Nature (London) **562**, 552 (2018).
[28] C.-E. Bardyn, T. Karzig, G. Refael, and T. C. H. Liew, Chiral Bogoliubov excitations in nonlinear bosonic systems, Phys. Rev. B **93**, 020502(R) (2016).
[29] O. Bleu, D. D. Solnyshkov, and G. Malpuech, Interacting quantum fluid in a polariton Chern insulator, Phys. Rev. B **93**, 085438 (2016).
[30] O. Bleu, D. D. Solnyshkov, and G. Malpuech, Photonic versus electronic quantum anomalous Hall effect, Phys. Rev. B **95**, 115415 (2017).
[31] D. Leykam and Y. D. Chong, Edge Solitons in Nonlinear-Photonic Topological Insulators, Phys. Rev. Lett. **117**, 143901 (2016).
[32] Y. Lumer, M. C. Rechtsman, Y. Plotnik, and M. Segev, Instability of bosonic topological edge states in the presence of interactions, Phys. Rev. A **94**, 021801(R) (2016).
[33] Y. Lumer, Y. Plotnik, M. C. Rechtsman, and M. Segev, Self-Localized States in Photonic Topological Insulators, Phys. Rev. Lett. **111**, 243905 (2013).
[34] M. J. Ablowitz, C. W. Curtis, and Y.-P. Ma, Linear and nonlinear traveling edge waves in optical honeycomb lattices, Phys. Rev. A **90**, 023813 (2014).
[35] Y. V. Kartashov and D. V. Skryabin, Modulational instability and solitary waves in polariton topological insulators, Optica **3**, 1228 (2016).
[36] D. R. Gulevich, D. Yudin, D. V. Skryabin, I. V. Iorsh, and I. A. Shelykh, Exploring nonlinear topological states of matter with exciton-polaritons: Edge solitons in Kagome lattice, Sci. Rep. **7**, 1780 (2017).
[37] C. Li, F. Ye, X. Chen, Y. V. Kartashov, A. Ferrando, L. Torner, and D. V. Skryabin, Lieb polariton topological insulators, Phys. Rev. B **97**, 081103(R) (2018).
[38] O. Bleu, G. Malpuech, and D. D. Solnyshkov, Robust quantum valley Hall effect for vortices in an interacting bosonic quantum fluid, Nat. Commun. **9**, 3991 (2018).
[39] Y. V. Kartashov and D. V. Skryabin, Bistable Topological Insulator with Exciton-Polaritons, Phys. Rev. Lett. **119**, 253904 (2017).
[40] X. Zhou, Y. Wang, D. Leykam, and Y. D. Chong, Optical isolation with nonlinear topological photonics, New J. Phys. **19**, 095002 (2017).
[41] K. Esaki, M. Sato, K. Hasebe, and M. Kohmoto, Edge states and topological phases in non-Hermitian systems, Phys. Rev. B **84**, 205128 (2011).
[42] H. Schomerus, Topologically protected midgap states in complex photonic lattices, Opt. Lett. **38**, 1912 (2013).
[43] J. M. Zeuner, M. C. Rechtsman, Y. Plotnik, Y. Lumer, S. Nolte, M. S. Rudner, M. Segev, and A. Szameit, Observation of a Topological Transition in the Bulk of a Non-Hermitian System, Phys. Rev. Lett. **115**, 040402 (2015).
[44] S. Weimann, M. Kremer, Y. Plotnik, Y. Lumer, S. Nolte, K. G. Makris, M. Segev, M. C. Rechtsman, and A. Szameit, Topologically protected bound states in photonic parity–time-symmetric crystals, Nat. Mater. **16**, 433 (2017).
[45] L. Pilozzi and C. Conti, Topological lasing in resonant photonic structures, Phys. Rev. B **93**, 195317 (2016).
[46] P. St-Jean, V. Goblot, E. Galopin, A. Lemaítre, T. Ozawa, L. Le Gratiet, I. Sagnes, J. Bloch, and A. Amo, Lasing in topological edge states of a 1D lattice, Nat. Photonics **11**, 651 (2017).
[47] M. Parto, S. Wittek, H. Hodaei, G. Harari, M. A. Bandres, J. Ren, M. C. Rechtsman, M. Segev, D. N. Christodoulides, and M. Khajavikhan, Edge-Mode Lasing in 1D Topological Active Arrays, Phys. Rev. Lett. **120**, 113901 (2018).
[48] H. Zhao, P. Miao, M. H. Teimourpour, S. Malzard, R. El-Ganainy, H. Schomerus, and L. Feng, Topological hybrid silicon microlasers, Nat. Commun. **9**, 981 (2018).
[49] B. Bahari, A. Ndao, F. Vallini, A. El Amili, Y. Fainman, and B. Kanté, Nonreciprocal lasing in topological cavities of arbitrary geometries, Science **358**, 636 (2017).
[50] G. Harari, M. A. Bandres, Y. Lumer, M. C. Rechtsman, Y. D. Chong, M. Khajavikhan, D. N. Christodoulides, and M. Segev, Topological insulator laser: Theory, Science **359**, eaar4003 (2018).
[51] M. A. Bandres, S. Wittek, G. Harari, M. Parto, J. Ren, M. Segev, D. N. Christodoulides, and M. Khajavikhan, Topological insulator laser: Experiment, Science **359**, eaar4005 (2018).
[52] C. Schneider, K. Winkler, M. D. Fraser, M. Kamp, Y. Yamamoto, E. A. Ostrovskaya, and S. Hofling, Exciton-polariton trapping and potential landscape engineering, Rep. Prog. Phys. **80**, 016503 (2017).
[53] A. V. Kavokin, J. J. Baumberg, G. Malpuech, and F. P. Laussy, *Microcavities* (Oxford University Press, Oxford, 2017).

[54] T. Jacqmin, I. Carusotto, I. Sagnes, M. Abbarchi, D. D. Solnyshkov, G. Malpuech, E. Galopin, A. Lemaítre, J. Bloch, and A. Amo, Direct Observation of Dirac Cones and a Flatband in a Honeycomb Lattice for Polaritons, Phys. Rev. Lett. **112**, 116402 (2014).

[55] M. Milicevic, T. Ozawa, P. Andreakou, I. Carusotto, T. Jacqmin, E. Galopin, A. Lemaitre, L. Le Gratiet, I. Sagnes, J. Bloch, and A. Amo, Edge states in polariton honeycomb lattices, 2D Mater. **2**, 034012 (2015).

[56] F. Baboux, L. Ge, T. Jacqmin, M. Biondi, E. Galopin, A. Lemaítre, L. Le Gratiet, I. Sagnes, S. Schmidt, H. E. Türeci, A. Amo, and J. Bloch, Bosonic Condensation and Disorder-Induced Localization in a Flat Band, Phys. Rev. Lett. **116**, 066402 (2016).

[57] C. E. Whittaker, E. Cancellieri, P. M. Walker, D. R. Gulevich, H. Schomerus, D. Vaitiekus, B. Royall, D. M. Whittaker, E. Clarke, I. V. Iorsh, I. A. Shelykh, M. S. Skolnick, and D. N. Krizhanovskii, Exciton-Polaritons in a Two-Dimensional Lieb Lattice with Spin-Orbit Coupling, Phys. Rev. Lett. **120**, 097401 (2018).

[58] S. Klembt, T. H. Harder, O. A. Egorov, K. Winkler, H. Suchomel, J. Beierlein, M. Emmerling, C. Schneider, and S. Höfling, Polariton condensation in S- and P-flatbands in a two-dimensional Lieb lattice, Appl. Phys. Lett. **111**, 231102 (2017).

[59] H. Flayac, I. A. Shelykh, D. D. Solnyshkov, and G. Malpuech, Topological stability of the half-vortices in spinor exciton-polariton condensates, Phys. Rev. B **81**, 045318 (2010).

[60] V. G. Sala, D. D. Solnyshkov, I. Carusotto, T. Jacqmin, A. Lemaitre, H. Terćas, A. Nalitov, M. Abbarchi, E. Galopin, I. Sagnes, J. Bloch, G. Malpuech, and A. Amo, Spin-Orbit Coupling for Photons and Polaritons in Microstructures, Phys. Rev. X **5**, 011034 (2015).

[61] S. Dufferwiel, F. Li, E. Cancellieri, L. Giriunas, A. A. P. Trichet, D. M. Whittaker, P. M. Walker, F. Fras, E. Clarke, J. M. Smith, M. S. Skolnick, and D. N. Krizhanovskii, Spin Textures of Exciton-Polaritons in a Tunable Microcavity with Large TE-TM Splitting, Phys. Rev. Lett. **115**, 246401 (2015).

[62] D. Bajoni, P. Senellart, E. Wertz, I. Sagnes, A. Miard, A. Lemaítre, and J. Bloch, Polariton Laser Using Single Micropillar GaAs–GaAlAs Semiconductor Cavities, Phys. Rev. Lett. **100**, 047401 (2008).

[63] C. Schneider, A. Rahimi-Iman, N. Young Kim, J. Fischer, I. G. Savenko, M. Amthor, M. Lermer, A. Wolf, L. Worschech, V. D. Kulakovskii, I. A. Shelykh, M. Kamp, S. Reitzenstein, A. Forchel, Y. Yamamoto, and S. Höfling, An electrically pumped polariton laser, Nature (London) **497**, 348 (2013).

[64] H. Deng, G. Weihs, C. Santori, J. Bloch, and Y. Yamamoto, Condensation of semiconductor microcavity exciton polaritons, Science **298**, 199 (2002).

[65] S. Kéna-Cohen and S. R. Forrest, Room-temperature polariton lasing in an organic single-crystal microcavity, Nat. Photonics **4**, 371 (2010).

[66] M. Wouters and I. Carusotto, Excitations in a Nonequilibrium Bose-Einstein Condensate of Exciton Polaritons, Phys. Rev. Lett. **99**, 140402 (2007).

[67] J. Keeling and N. G. Berloff, Spontaneous Rotating Vortex Lattices in a Pumped Decaying Condensate, Phys. Rev. Lett. **100**, 250401 (2008).

[68] I. Carusotto and C. Ciuti, Quantum fluids of light, Rev. Mod. Phys. **85**, 299 (2013).

[69] K. G. Lagoudakis, F. Manni, B. Pietka, M. Wouters, T. C. H. Liew, V. Savona, A. V. Kavokin, R. André, and B. Deveaud-Plédran, Probing the Dynamics of Spontaneous Quantum Vortices in Polariton Superfluids, Phys. Rev. Lett. **106**, 115301 (2011).

[70] M. Wouters, I. Carusotto, and C. Ciuti, Spatial and spectral shape of inhomogeneous nonequilibrium exciton-polariton condensates, Phys. Rev. B **77**, 115340 (2008).

[71] M. Wouters and I. Carusotto, Superfluidity and Critical Velocities in Nonequilibrium Bose-Einstein Condensates, Phys. Rev. Lett. **105**, 020602 (2010).

[72] M. Sich, F. Fras, J. K. Chana, M. S. Skolnick, D. N. Krizhanovskii, A. V. Gorbach, R. Hartley, D. V. Skryabin, S. S. Gavrilov, E. A. Cerda-Méndez, K. Biermann, R. Hey, and P. V. Santos, Effects of Spin-Dependent Interactions on Polarization of Bright Polariton Solitons, Phys. Rev. Lett. **112**, 046403 (2014).

[73] F. Baboux, D. De Bernardis, V. Goblot, V. N. Gladilin, C. Gomez, E. Galopin, L. Le Gratiet, A. Lemaitre, I. Sagnes, I. Carusotto, M. Wouters, A. Amo, and J. Bloch, Unstable and stable regimes of polariton condensation, Optica **5**, 1163 (2018).

[74] See Supplemental Material at http://link.aps.org/supplemental/10.1103/PhysRevLett.122.083902 for extended spectra of lattices with zigzag and bearded edges.

[75] Y. S. Kivshar and D. E. Pelinovsky, Self-focusing and transverse instabilities of solitary waves, Phys. Rep. **331**, 117 (2000).